Nanoscale

PAPER

View Article Online
View Journal

Cite this: DOI: 10.1039/d6nr00859c

DNA–cisplatin modified single-walled carbon nanotubes for the hydrogen evolution reaction

R. Hendi,[a] K. Englert,[b] James H. R. Tucker,[b] Alex P. G. Robinson[a] and Neil V. Rees*[a]

A three-component catalyst material has been developed for the hydrogen evolution reaction (HER) from preformed DNA–cisplatin (cisPt) adducts functionalised on single-walled carbon nanotubes (SWCNTs) under acidic conditions (pH 3). The DNA was used as a scaffold for platinum placement at ultra-low loadings, sourced from the anticancer drug cisplatin (cisPt). The SWCNTs were successfully functionalised with DNA, cisPt, and DNA–cisPt adducts, with each evaluated for their catalytic performance for HER. The dispersion efficiency of the nanotube functionalisation process was optimised as a function of the molar ratio of SWCNT to DNA–cisPt and the sonication time employed, with 1 : 1 and 45 minutes respectively proving optimal. Scanning Transmission Electron Microscopy (STEM) was used to study the resulting changes to the surface morphology for each condition. Overall, the reaction time of the functionalisation process had a greater influence on the resulting platinum nanocluster size than the employed molar ratio of SWCNT to DNA–cisPt. Cyclic voltammetry measurements revealed that the highest mass activity for the HER could be attained through functionalisation of SWCNTs with DNA–cisPt adducts as opposed to with cisPt alone, validating the essential role of DNA in this catalyst design. The activity was found to correlate to the Pt nanocluster size and distribution, which was optimal at a 1 : 1 molar ratio of SWCNT to DNA–cisPt. The importance of the role of both the DNA and the SWCNTs was validated *via* the mass activity measurements of the Pt, with the performance attained for the three-component SWCNT–DNA–cisPt catalyst (18.4 ± 0.9 mA mg^{-1}_{Pt}) being higher than that for SWCNT–cisPt (11.9 ± 0.6 mA mg^{-1}_{Pt}), DNA–cisPt (10.0 ± 0.5 mA mg^{-1}_{Pt}) and bulk cisPt (7.4 ± 0.4 mA mg^{-1}_{Pt}). The superior activity is consistent with optimized Pt dispersion in the 1 : 1 SWCNT to DNA–cisPt combination. While the measured nanocluster size of the three-component system (1.23 ± 0.65 nm) is statistically similar to that of SWCNT–cisPt (1.27 ± 0.46 nm) in the absence of DNA, the nucleic acid scaffold appears to promote more effective utilization of Pt active sites.

Received 2nd March 2026,
Accepted 28th March 2026

DOI: 10.1039/d6nr00859c

rsc.li/nanoscale

Introduction

Fuel cells represent a sustainable energy solution by converting the chemical energy in fuels like hydrogen into electricity through reactions with oxygen, producing only water as a by-product.[1] Hydrogen fuel cells are pivotal to achieving the carbon target by 2050;[2,3] however, large-scale commercialization is limited by material costs and challenges in hydrogen production, storage, and transportation.[4]

The process of electrochemical water splitting can provide a green and environmentally friendly means for an efficient and sustainable method for hydrogen production. The electrolysis of water, eqn (1), involves two half-cell reactions, the hydrogen evolution reaction (HER), eqn (2), and the oxygen evolution reaction (OER), eqn (3):

$$H_2O(l) \rightarrow H_2(g) + \frac{1}{2}O_2(g)\ \Delta E^\circ = 1.23\ \text{V}\ vs.\ \text{NHE} \quad (1)$$

HER

$$2H^+(aq) + 2e^- \rightarrow H_2(g) \quad (2)$$

OER

$$2H_2O(l) \rightarrow 4H^+(aq) + 4e^- + O_2(g). \quad (3)$$

To efficiently produce hydrogen, kinetic barriers can be minimized using suitable electrocatalysts such as the Platinum Group Metal (PGM)-based catalysts. Platinum is a particularly highly effective choice for HER, offering optimal hydrogen binding energy and lower activation energy. However, the high cost and scarcity of these PGMs remain the major obstacles to large-scale deployment of hydrogen-based fuel cells.[5] For

[a]School of Chemical Engineering, University of Birmingham, Birmingham B15 2TT, UK. E-mail: n.rees@bham.ac.uk
[b]School of Chemistry, University of Birmingham, Birmingham B15 2TT, UK

example, for a polymer electrolyte membrane fuel cell stack, the catalyst layer coated on its surface accounts for over 40% of the overall cost.[6] To overcome this issue, extensive research has focused on reducing the cost of electrocatalyst materials by minimizing platinum loading. Strategies include increasing the number of active Pt sites, decreasing the thickness of the catalyst layer to ≤25 μm, and synthesizing smaller Pt particles (<10 nm) dispersed on carbon supports.[7]

Support materials are also critical in enhancing the catalyst performance as they can facilitate a more uniform distribution of the Pt metal single-atom catalysts, resulting in an improvement in both metal utilization efficiency and reaction rate, since more of the Pt active sites become accessible.[5] Additionally, support materials can enhance catalyst durability by modifying the electronic environment of the active sites through strong metal–support interactions.[8] Carbon-based materials are the primary choice as support for Pt catalysts in proton exchange membrane fuel cells[9] as they offer both high electrical conductivity and porosity, large specific surface area, and strong interactions with the Pt.[10] Moreover, carbon supports allow for the recycling of spent Pt catalysts, contributing to a more sustainable use of this precious metal.[10]

Among alternative supports to conventional carbon-based materials, carbon nanotubes (CNTs) have emerged as promising candidates for further improving catalytic efficiency and reducing Pt loading.[7] Ultra-small Pt nanoparticles are particularly active for the HER; however, their high surface energy can lead to aggregation and loss of activity over time. Stabilization of these particles is essential, and one effective strategy involves anchoring them onto defect-rich substrates. Single-walled carbon nanotubes (SWCNTs) serve as ideal supports due to their high surface area, excellent electrical conductivity, and inherent chemical stability – attributes that have proven advantageous across a range of electrocatalytic applications including the effective stabilisation of ultra-small Pt nanoparticles, which are otherwise prone to aggregation due to their high surface energy.[7,11] CNTs can be functionalised using various methods, including electrochemical, physical/chemical deposition, both with and without surface activation, and electroless deposition, with or without reducing agents.[12] Dispersing CNTs from bundles is typically achieved *via* ultrasonication, which overcomes van der Waals interactions.[11] Metal deposition has been demonstrated on both functionalized and unfunctionalized CNTs. For example, Cu and Ag have been deposited on SWCNTs and MWCNTs *via* electroless methods without reducing agents[13–25] or alternatively, bare Pt or Au nanoparticles can spontaneously form on SWCNT sidewalls when immersed in metal salt solutions.[26] In fact, the integration of platinum nanoparticles with SWCNTs and MWCNTs is well reported,[13,15,17,18,22,24,25] particularly in relation to fuel cell applications like polymer exchange fuel cells, where Pt–CNT composites are employed to enhance nanoparticle adhesion, accessibility and dispersion for both the hydrogen evolution and oxygen reduction reactions.

With the aim of further reducing platinum metal loadings in catalytic materials for clean fuel and energy production, we previously proposed a novel synthetic biology approach to platinum nanostructure design involving the use of DNA as a scaffold to precisely position metal atoms.[27] The underlying hypothesis was that spacing individual platinum atoms along the DNA backbone would minimise undesirable nanoparticle clustering and increase the number of exposed active sites through the formation of multiple covalent adducts,[27] thereby enhancing the catalytic efficiency of the resulting material. In order to achieve a controlled interaction with low platinum loadings, the anticancer drug cisplatin (cisPt), $[Pt(NH_3)_2Cl_2]$, was employed as the platinum source due to its well-characterized ability to form strong covalent complexes with DNA.[28–32] This interaction primarily involves the formation of two intrastrand Pt–N bonds between adjacent guanine bases at the N7 position, though other mono- and bidentate purine adducts are also possible. The robustness of these covalent bonds is critical in producing catalyst precursors with individually and regularly spaced Pt atoms. Accordingly, we observed clear trends in HER catalytic performance as a function of platinum loading on DNA, highlighting the promise of this design strategy.[27]

Given these promising results, we next considered that the Pt distribution throughout the catalytic material might be further improved by employing SWCNTs as anchoring sites for the DNA–cisPt scaffold rather than a conventional carbon support. The employment of CNTs functionalised with DNA is not unprecedented, and has been reported for electrochemical applications[12,26,33–35] due to their high surface to volume ratio, fast heterogeneous charge transfer and electrochemical stability. Additionally, the combination of Pt nanoparticles with CNTs and DNA together has also been explored in various electrochemical applications, including DNA biosensors,[36] DNA-templated Pt nanoparticle synthesis on SWCNTs[28] and nanostructured sensor arrays.[37–39] Therefore, herein we present the preparation and study of a three-component hybrid nanostructured material, SWCNT–DNA–cisPt, as a catalyst for the Hydrogen Evolution Reaction (HER). To assess the effectiveness of this approach, control samples with SWCNTs functionalised with either cisPt alone or DNA alone were also prepared. For the SWCNT–DNA–cisPt system, different molar ratios of the SWCNT to DNA–cisPt were tested, with the electrocatalytic performance of each configuration evaluated. The results indicate improved catalytic performance in the HER in the form of higher mass activities for the three-component SWCNT system over the two-component control systems.

Results and discussion

Optimisation of the reaction conditions for the functionalisation process

The method used to prepare the three-component SWCNT catalyst functionalised with DNA–cisPt, as well as those with the individual adduct components alone, virgin salmon milt DNA and cisPt respectively, are described in the Experimental section provided in the SI. In order to prepare the three-com-

ponent system, first we re-prepared the DNA–cisPt catalyst according to our previously reported procedure,[27] choosing a DNA to cisPt molar ratio of 1 : 1 where our data had suggested that all purine nucleobases were coordinated *via* mono- or bidentate Pt–N adducts. We were able to reaffirm the reproducibility of the performance of the catalyst design at this Pt loading, recording a similar onset potential at a current density of 0.1 mA cm^{-2} (−0.6 V *vs.* SCE) and a similar mass activity (10 mA g^{-1}_{Pt}).

Noncovalent SWCNT functionalisation to prepare each catalyst followed the same procedure each time, which first involved SWCNT dispersion in a 50% v/v IPA aqueous solution through sonication for 90 minutes, followed by further sonication in the presence of either cisPt (1 : 1 molar ratio), DNA (1 : 1 molar ratio), or DNA–cisPt in an ice-water bath, with a range of conditions investigated for the latter (*vide infra*). DNA assemblies with CNTs are considered to be stabilised by π–π stacking interactions *via* adsorption of the hydrophobic nucleic bases of DNA onto the nanotube surface while the hydrophilic sugar–phosphate backbone of DNA is left exposed to the solvent,[33,34] which solubilises the nanostructure in water.[35] It is worth noting that our preparation differed from a related one reported by Ostojic *et al.*,[40] where SWCNTs were first wrapped with DNA, which was followed by binding with cisplatin and potassium tetrachloroplatinate complexes, which were then reduced to generate Pt nanoparticles on the DNA-encapsulated SWCNTs. Our approach takes advantage of the initial use of DNA to assemble and distribute the Pt complexes beforehand, with the DNA acting as a scaffold, followed by its interaction with the SWCNT support.

Several studies have investigated optimisation of dispersion of CNTs as a function of DNA sequence, DNA length, sonication time, type of CNT and solvent condition.[26,33–39] For this work, we identified two key experimental parameters as most likely affecting the size and distribution of Pt nanoparticles on the SWCNT support. The first was the sonication time used for the functionalisation reaction between the SWCNT and the DNA–cisPt adduct, and the second was the molar ratio between the reactants. To monitor the changes of these parameters, both the catalyst morphology and nanoparticle size was studied using STEM imaging, and the extent to which variations in each of these conditions impacted the electrocatalytic performance for the HER at pH 3 was explored using cyclic voltammetry. These parameters are crucial since the HER (eqn (2)) is sensitive to the size, shape and crystal facets of the Pt nanoparticles, which have a key role in determining the overall catalytic performance. In particular, the morphology of the Pt nanoparticles can expose different crystal planes, leading to different atomic arrangements on the catalyst surface of distinct electronic and geometric structures.[5]

Ultrasound sonication time. Both ultrasound energy density and sonication time have been shown to have a direct impact on carbon nanotube structure,[41] although the latter can result in greater nanotube damage upon prolonged sonication. The use of a broader sonicator tip or plate sonicators under such conditions would allow for more complete dispersions while minimizing damage.[41] Alternatively, combining experimental methods with theory *via* machine learning has been reported[42] as a tool for predicting the outcomes of varying these ultrasonication parameters (energy density, time, and device type), so that an optimal balance can be struck between effective dispersion and minimal damage to the nanotubes. Here, to study the effect of sonication time on the dispersion of the three-component SWCNT–DNA–cisPt system, a sufficiently large ratio of SWCNT catalyst support was used (*i.e.* 2 : 1 SWCNT : DNA–cisPt) to minimise substrate influence on catalyst distribution and size. Sonication times of 15, 30, 45 and 90 minutes were investigated. With the power input of the sonication probe being 130 W, the energy supplied increased from 117 kJ to 702 kJ as the sonication time increased from 15 to 90 minutes. Once synthesised, the samples were imaged under STEM to compare and contrast their morphologies and analyse both the size and distribution of the Pt particles within them.

The STEM imaging of the 2 : 1 SWCNT : DNA–cisPt catalyst showed evident changes in the distribution of the cisPt (*i.e.* Pt) on the SWCNT support as a function of sonication time (Fig. S4 in the SI). For example, as the sonication time increased from 15 to 90 minutes, the Pt distribution improved significantly due to the breaking up of agglomerated Pt structures, compared to the larger areas occupied by these Pt agglomerates at 15 minutes. The size of the area occupied by Pt agglomerates could be estimated using ImageJ software, as highlighted in Fig. S1, to reflect the distribution of Pt, *i.e.* the smaller the area, the better the Pt distribution. At 15 minutes, the average agglomerate size was 50.1 ± 24.2 nm (based on 11 measurements), while at 90 minutes it decreased to 12.3 ± 2.4 nm (based on 44 measurements, see Tables S2 and S3 in the SI). The large standard deviation at 15 minutes suggests that the sonication time was insufficient for achieving a uniform Pt distribution across the catalyst surface.

Representative regions showing a uniform distribution of Pt were selected to measure changes in Pt nanocluster size with sonication time. The average nanocluster size was determined from 30 to 161 measurements per condition (excluding single atoms) and Particle Size Distributions (PSDs) were constructed from these data (see Fig. S5–S8 in the SI). Fig. 1A suggests a possible trend towards improved Pt distribution and a consequently smaller nanoparticle size with increased sonication time. Notwithstanding the relatively large standard deviations (signal-to-noise being a particularly challenging issue), meaning that the observed changes in particle size must be interpreted with caution, a more notable reduction appears to occur between 15 and 30 minutes of sonication, where the average size decreases from 1.64 ± 0.76 nm to 1.32 ± 0.52 nm. Beyond 45 minutes, only marginal differences, if any, are found. Based on previous studies,[43] it could be the case that further increases in sonication time may result in one or a combination of the following competing processes taking place: (1) re-aggregation of the nanoclusters after their initial break up by sonication; (2) the defects on the SWCNTs acting as nucleation sites for Pt nanoparticle growth. The optimum sonication time was therefore concluded to be 45 minutes.

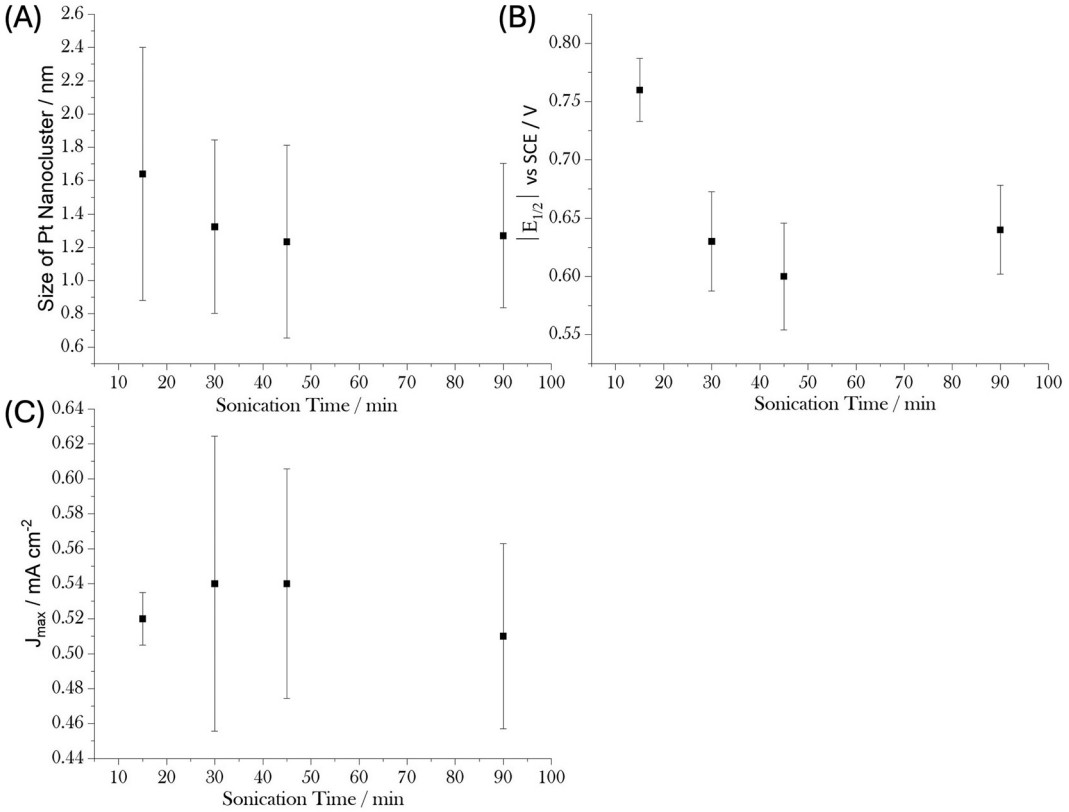

Fig. 1 The changes in the: (A) average platinum nanocluster size (diameter, nm), (B) (absolute) half wave potential ($E_{1/2}$), (C) maximum (cathodic) current density, J_{max} (mA cm^{-2}) with sonication time for the HER (1 mM $HClO_4$ and 0.1 m $NaClO_4$) pH = 3, at 50 mV s^{-1} for the 2 : 1 SWCNT : DNA–cisPt/Glassy Carbon (GC) modified working electrode surface. The data were derived from a minimum of 3 experiments.

The electrochemical behaviour of the 2 : 1 SWCNT : DNA–cisPt catalyst as a function of sonication time was investigated for the HER. Cyclic voltammograms in 1 mM $HClO_4$ and 100 mM $NaClO_4$ (pH 3) electrolyte solution for each sonication time (15, 30, 45 and 90 minutes) were run at a scan rate of 50 mV s^{-1}. The influence of sonication time on the electrocatalytic performance was measured as a function of the half-wave potential ($E_{1/2}$), which can be taken as a first approximation of the formal potential of the electrode[27] and the catalyst activity *i.e.* current density, J (mA cm^{-2}), which is measured based on the geometric surface area of the working electrode. For both of these parameters, an average (absolute) value was determined to construct a plot to correlate these results with sonication time, as shown in Fig. 1B and C respectively (the corresponding raw data are provided in Table S5 of the SI).

Comparing Fig. 1A and B, there is clearly a more pronounced change in $E_{1/2}$ with sonication time than with Pt nanocluster size for the first 30 minutes of sonication, with $E_{1/2}$ decreasing from 0.78 ± 0.02 V to 0.68 ± 0.02 V (*vs.* SCE). Beyond 45 minutes, the changes become less significant. As also found for the nanocluster size, the overall trend in catalyst activity (J_{max}) with sonication time, shown in Fig. 1C, must be treated with caution due to the large standard deviations. However, the data suggests that optimal activation conditions are reached by a sonication time of 45 minutes. This is an improvement from previous studies on the dispersion efficiency of CNTs by DNA with repeating thymine residues, poly$(T)_{30}$,[44] which found that sonication times higher than 90 minutes were required to obtain well-dispersed individual DNA-wrapped CNTs. Increasing the sonication time to 120 minutes increased the dispersion efficiency, but decreased the size of the CNTs, suggesting that they break during long sonication periods.[44]

Molar ratio of SWCNT : DNA–cisPt. Next the effect of different catalyst support loadings in the three-component catalyst system was investigated for Pt nanocluster size, half-wave potential ($E_{1/2}$) and the maximum current density (J_{max}). Four different molar ratios (x : 1, where x = 0.5, 1, 2, and 4) of SWCNT to DNA–cisPt were prepared and studied at the identified optimal sonication time of 45 minutes. Once again, the surface morphologies of the prepared materials were assessed using STEM imaging characterisation following the same methods described above. The average nanocluster size was found from the measurements (single atoms were excluded from the analysis), from which the particle size distributions (PSD) were constructed for each of the different catalysts fabricated, as provided in Fig. S5–S8 in the SI. It was expected that increasing the ratio of SWCNT to DNA–cisPt should result in an improved Pt distribution (*i.e.* smaller Pt nanoclusters), due to the larger surface area available to support the DNA–cisPt catalyst. However, the results showed that increasing the ratio

beyond 1 : 1 resulted in no significant change in the nanocluster size, *i.e.* 1.23 ± 0.65 nm at 1 : 1 *vs.* 1.23 ± 0.58 nm at 2 : 1 SWCNT : DNA–cisPt (Fig. 2A), indicating that a ratio of 1 : 1 catalyst to support was sufficient for achieving an optimum distribution of the Pt nanoclusters for these reaction conditions.

The electrochemical behaviour of the x : 1 SWCNT : DNA–cisPt catalyst was also evaluated as a function of molar ratio of the SWCNT to DNA–cisPt for the HER, in 1 mM $HClO_4$ and 100 mM $NaClO_4$ using cyclic voltammetry at a voltage scan rate of 50 mV s^{-1}. The resulting half-wave potential ($E_{1/2}$) and maximum current density values (J_{max}) (mA cm^{-2}) are displayed in Fig. 2B and C respectively. Notwithstanding the large standard deviation for the 1 : 1 ratio, a correlation is apparent between the molar ratio of the SWCNT : DNA–cisPt and the $E_{1/2}$ value, with a minimum value observed at a ratio of 2 : 1. In terms of electrocatalytic activity, increasing the molar ratio of the SWCNT : DNA–cisPt from 0.5 : 1 to 1 : 1 reveals an enhancement in the average current density, reaching a maximum of approximately 650 μA cm^{-2}. However, further increases in the ratio to 2 : 1 and 4 : 1 give a decline in the average activity, with current densities plateauing around 50 μA cm^{-2}. This trend is consistent with the minimal changes observed in Pt nanocluster size beyond the 1 : 1 ratio.

Overall, while the initial increase in SWCNT content likely improves conductivity and facilitates better Pt dispersion, further additions appear to dilute the presence of the Pt active sites, resulting in a less favourable performance (J_{max}). These findings suggest that a 1 : 1 SWCNT : DNA–cisPt ratio at a sonication time of 45 minutes provides an optimal balance between catalyst to support loading, enabling efficient Pt dispersion and maximal catalytic activity. This is in agreement with previous observations made by Taeger *et al.*,[45] who found that the best dispersion efficiency is achieved at DNA : CNT ratios of 1 : 1 or 1 : 2, while the latter minimizes the amount of unbound DNA. A catalyst size of 1.23 ± 0.65 nm achieved at a 1 : 1 molar ratio of SWCNT to cis-Pt suggests that a sufficient number of active catalytic centres are available to accept protons for the HER, which requires on average 5 platinum atoms for the reduction of the protons to molecular hydrogen[20] (in acidic conditions). However, the direct correlation between catalyst size and catalytic performance is a challenging phenomenon, since decreasing the particle size can also change the electronic properties and shape of the particles

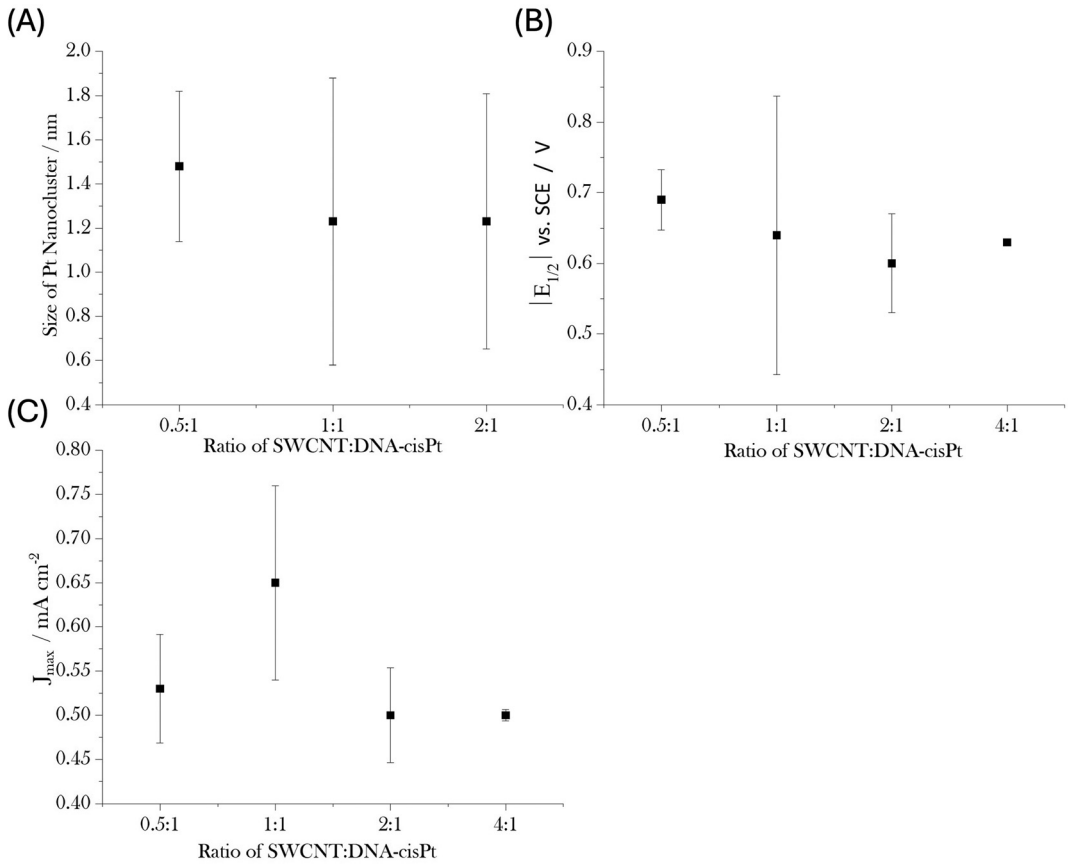

Fig. 2 The changes in the: (A) average platinum nanocluster size (diameter, nm) (B) (absolute) half wave potential ($E_{1/2}$), (C) maximum (cathodic) current density, J_{max} (mA cm^{-2}) with the ratio of (x : 1) SWCNTs to DNA–cisPt/GC working electrode prepared at the optimum sonication time of 45 minutes for the HER (1 mM $HClO_4$ and 0.1 M $NaClO_4$) pH 3, at 50 mV s^{-1}. The average J_{max}, $E_{1/2}$ and standard deviation errors were calculated using a minimum of 3 datapoints.

and consequently catalytic behaviour. For example, for particle sizes made up of ≤100 atoms, a 'non-scalable regime' is reached, where drastic changes are observed with each atom removed.[46] Even then, when ultra-low loadings of Pt are used for the HER/HOR (in acidic conditions), the mass-transport limitations of the reaction make the assessment of true intrinsic activity of Pt challenging, as described elsewhere.[47] Therefore a true ideal catalyst size may be difficult to find and instead for Pt nanoclusters, a maximum in mass-specific activity is measured for particle sizes between 1.5 nm and 3.0 nm.[46]

Comparison of morphology and particle size distribution

With the optimal reaction conditions identified for the functionalization process of the SWCNT support with DNA–cisPt, *i.e.* a sonication time of 45 minutes and a molar ratio of 1 : 1 of support to catalyst, it was decided to conduct comparative studies involving other Pt-containing materials (SWCNT–cisPt, DNA–cisPt and cisPt alone) to establish the effect of different catalyst configurations on morphology and particle size distribution.

To begin with, STEM imaging and particle size distribution (PSD) analyses were performed to examine the morphology and dispersion of Pt on the SWCNTs, with the PSD provided in the SI. During STEM imaging, no noticeable migration or sintering of Pt atoms was observed under a 200 keV electron beam, suggesting strong immobilization of Pt on the SWCNT surface. Fig. 3A shows the starting SWCNTs free of metallic impurities, providing a high surface area that facilitates effective Pt dispersion and enhances the accessibility of active sites. Fig. 3B–F demonstrate that both Pt single atoms and nanoclusters of varying sizes can be observed in each of the catalysts prepared. The SWCNTs have packed together in an ordered arrangement to form a bundle, with numerous Pt nanoparticles dispersed along these bundles following the functionalisation process with cisPt (Fig. 3A *vs.* 3D). To gain insight into the Pt particle size and distribution on the SWCNTs, higher magnifications were employed to focus more closely on these bundles to visualise the Pt nanoparticles and atoms. The average nanocluster size for each material was calculated using at least 50 data points (excluding single atoms), and Particle Size Distributions (PSDs) were subsequently constructed from these data.

The effect of using SWCNTs as a support material for the DNA–cisPt can be better understood by comparing the nanoparticle size distribution of the Pt before and after the SWCNT functionalisation process. For example, in the case of the DNA–cisPt complex, a visibly reduced degree of agglomeration was observed after functionalization with SWCNTs (Fig. 3B *vs.* 3C, corresponding to with *vs.* without functionalisation respectively), indicating a more uniform distribution of Pt. This improved dispersion is further supported by the

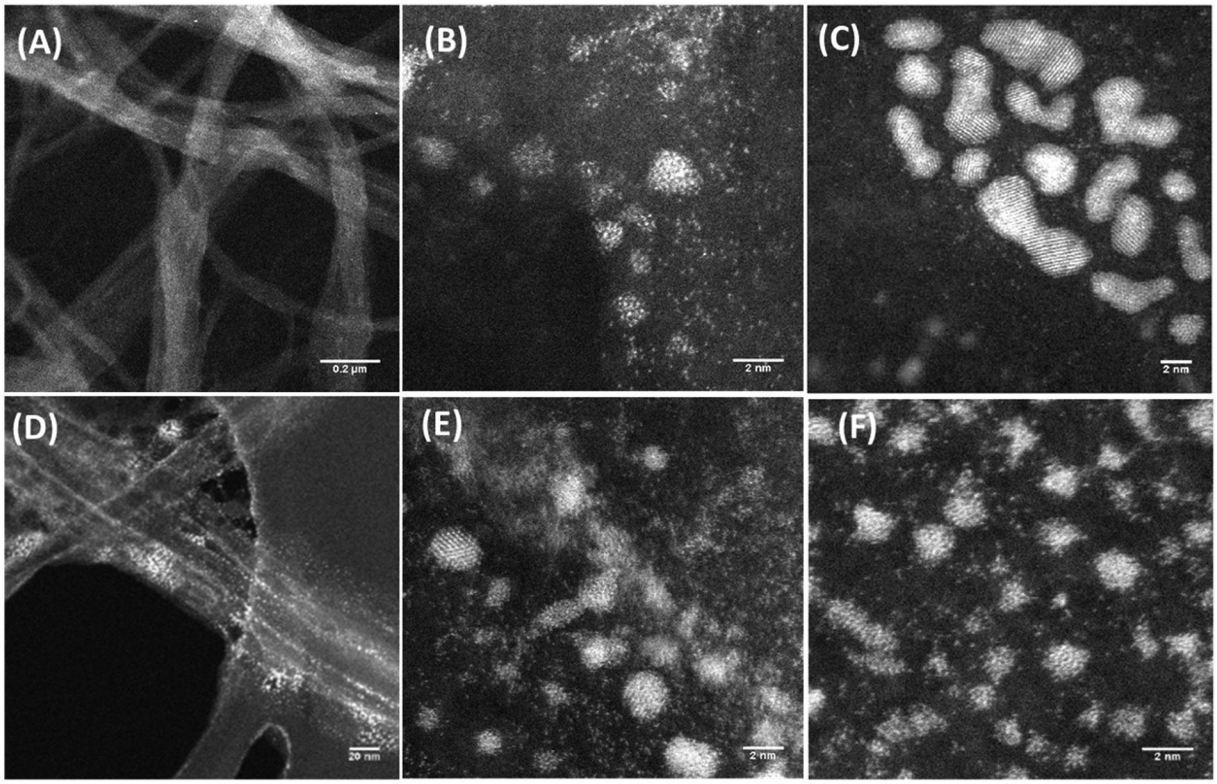

Fig. 3 HAADF STEM images of (A) SWCNT × 100k magnification, (B) SWCNT–DNA–cisPt (1 : 1 molar ratio) × 10 million magnification, (C) DNA–cisPt × 600k magnification, (D and E) SWCNT–cisPt × 100k and × 3 million magnification respectively, (F) cisPt (1 mM) × 8 million magnification. All films were drop cast from 3 µL solutions of holey carbon TEM grids.

reduction in average Pt nanocluster size, which decreased from 1.77 ± 0.86 nm to 1.23 ± 0.65 nm following SWCNT functionalization (see SI), although the large standard deviations must again be noted. In the case of bulk cisPt, a higher ratio of single atoms to nanoclusters was observed following SWCNT functionalization (1 mM, at a molar ratio of 1 : 1) as shown in Fig. 3E *vs.* 3F, again suggesting reduced Pt clustering and a better distribution of the Pt in the presence of the catalyst support. Interestingly, the functionalisation process of SWCNT with DNA–cisPt adducts indicated a higher ratio of atoms to clusters compared to that in the absence of DNA (Fig. 3B *vs.* 3E). However, both processes resulted in similar average Pt nanocluster sizes (1.23 ± 0.65 nm *vs.* 1.27 ± 0.46 nm respectively).

Comparison of electrocatalytic performance towards the HER

Voltammetric responses towards the HER for the various candidate materials cast on glassy carbon (GC) are presented in Fig. 4A. The potential (E) is a fundamental parameter in electrocatalysis; however, the rate of the reaction does not necessarily increase uniformly across different potentials. In other words, the reaction rate at potential E_1 may differ significantly from that at E_2, even if both are within the same operational range. Hence, for comparison of the catalysts explored in this study, the potential required to achieve a current density of −0.1 mA cm^{-2} *vs.* SCE (Fig. 4B) was selected as a benchmark for evaluating electrocatalytic performance. In addition, the mass activity (mA mg^{-1}_{pt}) of the catalyst film based on the Pt loading on the working electrode surface (see Table S1 in SI) was obtained to draw further comparisons, as illustrated in Fig. 4C.

A comparison of the materials in the absence of platinum revealed some interesting trends. Functionalization of SWCNTs with DNA resulted in a better electrocatalytic response towards the HER when compared to DNA alone. This is evidenced by a less negative onset potential required to reach a current density of 0.1 mA cm^{-2}, shifting from −1.4 V for DNA to −1.1 V (*vs.* SCE) for SWCNT–DNA, as shown in Fig. 4B. This improvement may be due to changed charge transfer kinetics facilitated by the sp^2 hybridized carbon bonds within the CNTs. However, when comparing SWCNT to the SWCNT–DNA, the latter exhibited a more negative onset potential. This can be attributed to the inherently low conductivity of DNA,[17] which reduces the efficiency of electron transfer between the catalyst film (SWCNT–DNA) on the electrode surface and the H^+ redox probe in solution.

On the other hand, functionalisation of SWCNTs with cisPt enhanced their electrochemical response, lowering the onset potential (at a current density of 0.1 mA cm^{-2}) from −0.81 V to −0.60 V (*vs.* SCE) (Fig. 4B). This shifts the catalyst behaviour

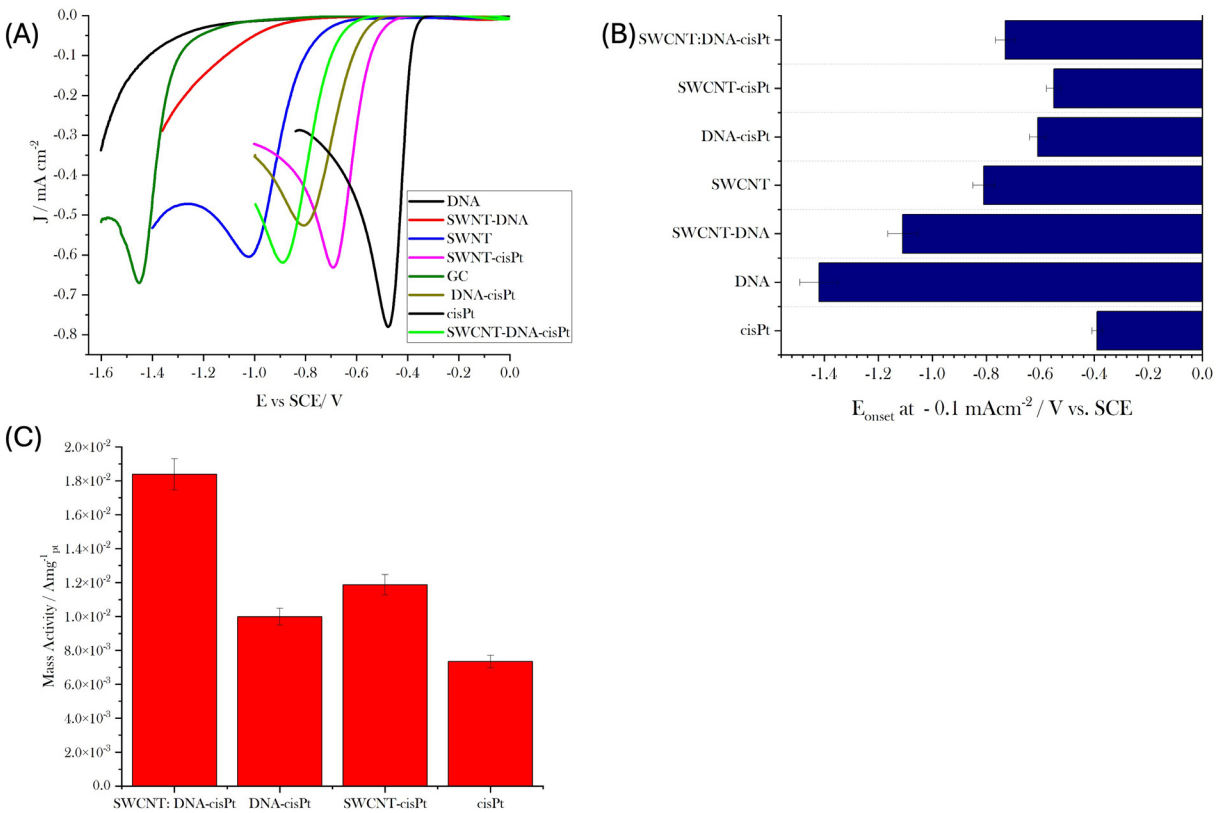

Fig. 4 (A) Voltammetry response for the HER for seven materials including SWCNT–DNA–cisPt (1 : 1 molar ratio) cast on glassy carbon (GC) (d = 3 mm) at 50 mV s^{-1} (1 mM $HClO_4$, 0.1 M $NaClO_4$); (B) absolute onset potential at −0.1 mA cm^{-2} for the named catalyst; (C) the corresponding average mass activity of the catalyst defined based on its Pt content for the HER.

closer towards that of bulk cisPt, which exhibited the lowest onset potential of −0.40 V *vs.* SCE (Fig. 4B). This favourable change in the electrocatalytic performance of the SWCNT can be better understood by looking at the electron transfer that takes place upon the deposition of Pt nanoparticles onto carbon nanotubes, which has been well reported.[17] The process involves the provision of 5d electrons to the nanotubes' valence band, increasing the electron density at the Fermi level.[17] Furthermore, Dobrzańska-Danikiewicz *et al.*[17] reported that the hybridization state of carbon in Pt-decorated CNTs remained unchanged with varying Pt concentrations.[17] We propose this as an explanation for our observations, in which bulk cisPt outperforms SWCNT–cisPt despite the latter exhibiting better Pt distribution. Functionalisation of cisPt with SWCNT, DNA, or both these materials (in the case of the three-component catalyst 1 : 1 SWCNT : DNA–cisPt), raises the onset potential in turn, with the latter giving the highest value of −0.72 V (Fig. 4B). However in terms of mass activity of Pt, the three-component SWCNT–DNA–cisPt catalyst exhibited the highest performance (18.4 ± 0.9 mA mg^{-1}_{Pt}) followed SWCNT–cisPt (11.9 ± 0.6 mA mg^{-1}_{Pt}), DNA–cisPt (10.0 ± 0.5 mA mg^{-1}_{Pt}) and bulk cisPt (7.4 ± 0.4 mA mg^{-1}_{Pt}).

In order to explain this superior activity for the three-component system, it is worth noting that the measured average Pt nanocluster size (1.23 ± 0.65 nm) for this assembly is statistically the same as that in SWCNT–cisPt (1.27 ± 0.46 nm), showing that the significant enhancement in the electrocatalytic response cannot be due to differences in nanocluster size. Instead, the enhancement is most likely due to a synergistic effect of the DNA, in anchoring Pt atoms, and the SWCNTs, in enhancing the dispersion of the Pt–DNA adducts respectively, consistent with previous reports.[40,48] In one particular previous example involving Pt and DNA,[48] improved electrocatalytic activity for the oxygen reduction reaction for a Pt/DNA–graphene oxide (GO) composite was found to arise from Pt–GO interactions that tuned the Pt d-electron density and strong DNA–GO binding that boosted conductivity and corrosion resistance, enabling faster transport of reaction species. The Pt nanoparticles were additionally stabilized by coordination to purine moieties in DNA and to graphene. In our case, the DNA scaffold appears to promote more effective utilization of Pt active sites, consistent with the enhanced mass activity of the Pt metal measurements.

These new findings validate the use of DNA as a means of anchoring the Pt atoms and nanoclusters at ultra-low loadings, as demonstrated in our previous work,[27] while the SWCNT acts as a high surface area support that provides defect sites to improve the dispersion and localisation of Pt atoms. STEM imaging characterisation further validates the effectiveness of this catalyst design, as much less agglomeration can be observed in the SWCNT–DNA–cisPt catalyst compared with DNA–cisPt alone. Importantly, the absence of DNA, as in the material SWCNT–cisPt, leads to a reduced mass activity of the Pt, highlighting the critical role of DNA in improving Pt site accessibility.

Conclusion

In this study, we present a simple, non-covalent strategy for functionalizing single-walled carbon nanotubes (SWCNTs) with a DNA–cisPt complex to fabricate an efficient platinum-based electrocatalyst for the hydrogen evolution reaction (HER) under acidic conditions (pH 3). DNA acts as a molecular scaffold to effectively disperse Pt atoms *via* their complexation as cisPt adducts, before exposure to the SWCNT support, with this approach outperforming the direct functionalisation of cisPt in the absence of DNA. Optimal conditions were achieved with 45 minutes of sonication for the functionalisation process and a 1 : 1 molar ratio of SWCNT to DNA–cisPt, resulting in the highest Pt mass activity (18.4 mA mg^{-1}_{Pt}), among all tested configurations.

These results validate the effectiveness of the initial catalyst design proposed which uses DNA for Pt anchoring and the SWCNTs as a high surface area support for these structures, with defect sites to localize the Pt atoms. STEM analysis confirmed that even though the average Pt nanocluster size is comparable to that obtained when cisPt is directly dispersed on to SWCNTs, the inclusion of DNA is key for achieving an enhanced performance of the Pt, as evidenced by the higher mass activity. This highlights the crucial role of DNA in enhancing Pt site accessibility, which is indicative of a synergistic effect, extending beyond solely a catalyst dispersion effect.

This work presents an innovative and simple approach for fabricating precious metal-based electrocatalysts, with our findings providing evidence for the crucial role of DNA in improving Pt surface accessibility and HER activity, outperforming SWCNTs alone. The improved utilization of this precious metal at ultra-low loadings, as evidenced by the mass activity measurements, is of significance for advancing fuel cell technologies and sustainable energy systems. Future work may focus on pretreatment of the DNA scaffold to enhance its electrical conductivity and exploring even lower Pt loadings to further lower material costs while maintaining or improving catalytic performance.

Conflicts of interest

There are no conflicts to declare.

Data availablity

All data supporting the findings of this study are provided in the supplementary information (SI). Supplementary information: electrochemical data, microscopy images, particle size distribution and XPS spectra. See DOI: https://doi.org/10.1039/d6nr00859c.

Acknowledgements

The authors wish to thank the DSTL for the award of a PhD studentship through CDE funding to K. E. (project title: DNA

Origami Catalysts, contract number: DSTLX-1000098487). The School of Chemical Engineering is also acknowledged for the award of a PhD studentship to R. H. The Centre for Chemical and Materials Analysis in the School of Chemistry is acknowledged for technical support.

References

1 S. Iijima, *Nature*, 1991, **354**, 56–58.
2 S. Z. Al Sheheri, Z. M. Al-Amshany, Q. A. Al Sulami, N. Y. Tashkandi, M. A. Hussein and R. M. El-Shishtawy, *Des. Monomers Polym.*, 2019, **22**, 8–53.
3 R. Atif and F. Inam, *Beilstein J. Nanotechnol.*, 2016, **7**, 1174–1196.
4 B. Ribeiro, E. C. Botelho, M. L. Costa and C. F. Bandeira, *Polímeros*, 2017, **27**, 247–255.
5 J. Zhu, L. Hu, P. Zhao, L. Y. S. Lee and K. Y. Wong, *Chem. Rev.*, 2020, **120**, 851–918.
6 J. H. Wee, K. Y. Lee and S. H. Kim, *J. Power Sources*, 2007, **165**, 667–677.
7 R. Dubey, D. Dutta, A. Sarkar and P. Chattopadhyay, *Nanoscale Adv.*, 2021, **3**, 5722–5744.
8 R. Balgis, G. M. Anilkumar, S. Sago, T. Ogi and K. Okuyama, *J. Power Sources*, 2012, **203**, 26–33.
9 J. Ma and Y. Sahai, *Electrochem. Commun.*, 2013, **30**, 63–66.
10 Y. J. Wang, N. Zhao, B. Fang, H. Li, X. T. Bi and H. Wang, *Chem. Rev.*, 2015, **115**, 3433–3467.
11 H. Cui, X. Yan, M. Monasterio and F. Xing, *Nanomaterials*, 2017, **7**, 106.
12 L. Qu and L. Dai, *J. Am. Chem. Soc.*, 2005, **127**, 10806–10807.
13 Q. Wang, N. Dai, J. Zheng and J. P. Zheng, *J. Electroanal. Chem.*, 2019, **854**, 113581.
14 C. Luo, H. Xie, Q. Wang, G. Luo and C. Liu, *J. Nanomater.*, 2015, 216439.
15 T. Rajala, R. Kronberg, R. Backhouse, M. E. M. Buan, M. Tripathi, A. Zitolo, *et al.*, *Appl. Catal., B*, 2020, **265**, 118589.
16 V. S. Thoi, R. E. Usiskin and S. M. Haile, *Chem. Sci.*, 2015, **6**, 1570–1577.
17 A. Dobrzańska-Danikiewicz, D. Łukowiec and J. Kubacki, *J. Nanomater.*, 2016, 8372315.
18 H. Tang, T. Kojima, K. Kazumi, K. Fukami and H. Sakaguchi, *ACS Omega*, 2024, **9**, 21378–21387.
19 T. Matsumoto, T. Komatsu, K. Arai, T. Yamazaki, M. Kijima, H. Shimizu, *et al.*, *Chem. Commun.*, 2004, **40**, 840–841.
20 E. A. Nagelli, F. J. Burpo, D. A. Marbach, A. N. Romero, D. J. Rabbia, H. W. Mahr, *et al.*, *J. Compos. Sci.*, 2020, **4**, 145.
21 W. Zhang, J. Chen, G. F. Swiegers, Z. F. Ma and G. G. Wallace, *Nanoscale*, 2010, **2**, 282–286.
22 M. Tavakkoli, N. Holmberg, R. Kronberg, H. Jiang, J. Sainio, E. I. Kauppinen, *et al.*, *ACS Catal.*, 2017, **7**, 3121–3130.
23 L. Cozzarini, G. Bertolini, S. T. Šuran-Brunelli, A. Radivo, M. V. Bracamonte, C. Tavagnacco, *et al.*, *Int. J. Hydrogen Energy*, 2017, **42**, 18763–18773.
24 C. Bittencourt, M. Hecq, A. Felten, J. J. Pireaux, J. Ghijsen, M. P. Felicissimo, *et al.*, *Chem. Phys. Lett.*, 2008, **462**, 260–264.
25 M. M. Waje, X. Wang, W. Li and Y. Yan, *Nanotechnology*, 2005, **16**, 2136–2140.
26 H. C. Choi, M. Shim, S. Bangsaruntip and H. Dai, *J. Am. Chem. Soc.*, 2002, **124**, 9058–9059.
27 K. Englert, R. Hendi, P. H. Robbs, N. V. Rees, A. P. G. Robinson and J. H. R. Tucker, *Nanoscale Adv.*, 2020, **2**, 4491–4497.
28 L. Dong, *Nanotechnology*, 2009, **20**, 465602.
29 E. R. Jamieson and S. J. Lippard, *Chem. Rev.*, 1999, **99**, 2467–2498.
30 B. J. Pages, D. L. Ang, E. P. Wright and J. R. Aldrich-Wright, *Dalton Trans.*, 2015, **44**, 3505–3526.
31 A. L. Pinto and S. J. Lippard, *Biochim. Biophys. Acta*, 1985, **780**, 167–180.
32 M. Sirajuddin, S. Ali and A. Badshah, *J. Photochem. Photobiol., B*, 2013, **124**, 1–19.
33 S. Daniel, T. P. Rao, K. S. Rao, S. U. Rani, G. R. K. Naidu, H. Y. Lee and T. Kawai, *Sens. Actuators, B*, 2007, **122**, 672–682.
34 L. Santiago-Rodríguez, G. Sánchez-Pomales and C. R. Cabrera, *Isr. J. Chem.*, 2010, **50**, 277–290.
35 D. Pramanik and P. K. Maiti, *ACS Appl. Mater. Interfaces*, 2017, **9**, 35287–35296.
36 N. Zhu, Z. Chang, P. He and Y. Fang, *Anal. Chim. Acta*, 2005, **545**, 21–26.
37 H. C. Su, M. Zhang, W. Bosze and J. H. Lim, *Nanotechnology*, 2013, **24**, 505501.
38 A. Paul, B. Bhattacharya and T. K. Bhattacharyya, *IEEE Trans. Nanotechnol.*, 2014, **13**, 335–342.
39 Y. Zhou, Y. Fang and R. P. Ramasamy, *Sensors*, 2019, **19**, 392.
40 G. N. Ostojic, J. R. Ireland and M. C. Hersam, *Langmuir*, 2008, **24**, 9784–9789.
41 H. Rennhofer and B. Zanghellini, *Nanomaterials*, 2021, **11**, 2091.
42 C. Glaubitz, B. Rothen-Rutishauser, M. Lattuada, S. Balog and A. Petri-Fink, *Nanoscale*, 2022, **14**, 12940–12950.
43 C. Hu, Y. Zhang, G. Bao, Y. Zhang, M. Liu and Z. L. Wang, *J. Phys. Chem. B*, 2005, **109**, 20072–20076.
44 R. Lahiji, B. D. Dolash, D. E. Bergstrom and R. Reifenberger, *Small*, 2007, **3**, 1912–1920.
45 S. Taeger, L. Y. Xuang, K. Günther and M. Mertig, *AIP Conf. Proc.*, 2005, **786**, 262–265.
46 J. Klein, A. K. Engstfeld, S. Brimaud and R. J. Behm, *Phys. Chem. Chem. Phys.*, 2020, **22**, 19059–19068.
47 J. N. Hansen, H. Prats, K. K. Toudahl, N. M. Secher, K. Chan and J. Kibsgaard, *ACS Energy Lett.*, 2021, **6**, 1175–1180.
48 J. N. Tiwari, K. Nath, S. Kumar, R. N. Tiwari, K. C. Kemp, N. H. Le, D. H. Youn, J. S. Lee and K. S. Kim, *Nat. Commun.*, 2013, **4**, 2221.